Effect of Roughness and Unsteadiness on the Performance of a New Low Pressure Turbine Blade at Low Reynolds Numbers

Francesco Montomoli

Howard Hodson

Whittle Laboratory,
University of Cambridge,
Cambridge, CB3 0DY, UK

Frank Haselbach

Rolls-Royce plc.,
Derby, DE24 8BJ, UK

This paper presents a study of the performance of a high-lift profile for low pressure turbines at Reynolds numbers lower than in previous investigations. By following the results of Coull et al. (2008, "Velocity Distributions for Low Pressure Turbines," ASME Paper No. GT2008-50589) on the design of high-lift airfoils, the profile is forward loaded. The separate and combined effects of roughness and wake passing are compared. On a front loaded blade, the effect of incidence becomes more important and the consequences in terms of cascade losses, is evaluated. The experimental investigation was carried out in the high speed wind tunnel of Whittle Laboratory, University of Cambridge. This is a closed-circuit continuous wind tunnel where the Reynolds number and Mach number can be fixed independently. The unsteadiness caused by wake passing in front of the blades is reproduced using a wake generator with rotating bars. The results confirm that the beneficial effect of unsteadiness on losses is present even at the lowest Reynolds number examined ($Re_3 = 20{,}000$). This beneficial effect is reduced at positive incidence. With a front loaded airfoil and positive incidence, the transition occurs on the suction side close to the leading edge and this results in higher losses. This has been found valid for the entire Reynolds range investigated ($20{,}000 \leq Re_3 \leq 140{,}000$). Roughening the surface also had a beneficial effect on the losses but this effect vanishes at the lower Reynolds numbers, i.e., ($Re_3 \leq 30{,}000$), where the surface becomes hydraulically smooth. The present study suggests that a blade with as-cast surface roughness has a lower loss than a polished one. [DOI: 10.1115/1.3148475]

1 Introduction

There is a need for airplanes that are cleaner, safer, and more affordable. To improve the fuel consumption and emissions, several different solutions have been proposed, with new wing shapes, lighter airplanes, and more efficient engines being particularly important. A significant improvement can be achieved by reducing the weight of the low pressure turbine, which currently represents up to 30% of the weight of the complete engine. As shown by Vazquez et al. [1], this reduction can be obtained by decreasing the number of blades. However, in order to have the same work, the aerodynamic loading of each blade has to be increased, which may have a detrimental effect on the efficiency. As shown by Hourmouziadis [2], the main difficulty encountered in the design of high-lift profiles is the control and reduction in the laminar separation bubble on the suction side due to high levels of deceleration on the rear of the suction surfaces, especially at low Reynolds numbers.

Schulte and Hodson [3] found that the unsteady environment in low pressure turbines, which is mainly due to the wakes of upstream blade rows convecting through downstream blade rows, has a beneficial effect on high-lift profiles. This is primarily due to the suppression of the separation bubble on the suction side. This suggested a new philosophy for the design of low pressure turbine blades: highly loaded profiles taking into account the wake passing in the design process [3,4].

The high-lift philosophy evolved to a point where, due to the high loading coefficient, the wake passing alone was not able to reduce or suppress the separation bubble. For this reason many authors have investigated new control methods, both passive [5–7] and active [10]. The main idea is to promote the transition before the laminar separation, thus reducing the losses on the blade suction side. The region of interest is located between the suction peak and the start of the separation bubble. Upstream of this region, the strong acceleration and low Reynolds number inhibits the transition. Downstream, there is no advantage because the boundary layer becomes turbulent due to the transition process in the shear layer of the separated flow. As shown by Roman and Howell [9] it is possible to promote transition using roughness elements, thus obtaining more lift with the same level of losses. Zhang and Hodson [5] compared different roughness levels and positions of the roughness to find the optimum in terms of losses. The studies accomplished by Zhang et al. [6] and Vera et al. [7] showed how passive and active methods can be used to reduce or suppress the separation bubble on the suction side.

Bloxham et al. [10] showed the effect of active flow control on high-lift profile. In particular, by controlling the phase between wake passing and jets, it is possible to obtain a further reduction in terms of losses. One of the main problems of using active control is concerned with their reliability in the harsh environment of a real gas turbine.

As core size reduces, new aircraft engines tend to have low pressure turbines with blades that have a reduced chord. This adds to the significance of the separation bubble in terms of the profile loss and the problems of controlling this with wakes alone. At the same time there is a growing interest in high altitude flights. The small size of the engines used for these applications and the low density of air at high altitude, require blades that are able to operate at very low Reynolds numbers.

By following the results obtained by Coull et al. [11] a new

Contributed by the International Gas Turbine Institute of ASME for publication in the JOURNAL OF TURBOMACHINERY. Manuscript received September 11, 2008; final manuscript received February 15, 2009; published online April 5, 2010. Review conducted by David Wisler. Paper presented at the ASME Turbo Expo 2008: Land, Sea and Air (GT2008), Berlin, Germany, June 9–13, 2008.

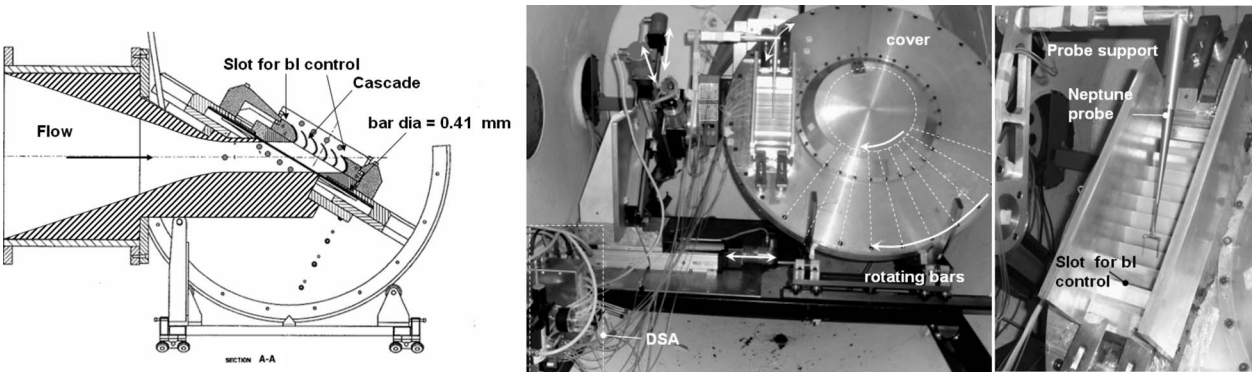

Fig. 1 View of high speed wind tunnel: (left) cross section; (right) photograph taken looking toward the inlet

high-lift profile has been designed. The airfoil is experimentally investigated with "as-cast" and polished surface finished, at Reynolds number lower than in previous investigations. For high-lift and ultra high-lift blades, it will be shown that there is an advantage in terms of the aerodynamic losses (and costs) by using a blade with an as-cast surface finish, and this will be shown in this paper. By considering that the optimum in terms of the loss at the design inlet flow angle is achieved by using a front loaded profile, the incidence effect has been also evaluated.

2 Experimental Apparatus

The experiments were performed using the transonic wind tunnel of the Whittle laboratory. This is a continuous closed-circuit tunnel with variable density, so that the Reynolds and Mach numbers can be fixed independently. To reach the Reynolds numbers required for this campaign, the vacuum system has been upgraded. Three vacuum pumps, working in parallel are now available to create subatmospheric inlet stagnation pressures as low as 7000 Pa absolute. A compressor controls the pressure ratio and the Mach number in the circuit. Before entering the cascade, the air passes through a honeycomb and screen and is then accelerated in a convergent nozzle. At the exit of the cascade, it is discharged into the large exit plenum that contains the test section. The inlet free stream turbulence is about 0.5%.

The presence of the wakes shed from an upstream blade row is simulated using a wake generator. The high speed bar wake generator consists of 60 cylindrical metal bars equally spaced at the outer periphery of a disk that rotates in a plane parallel to the leading edge plane of the cascade. Compared with a moving belt system, the circumferential speed of the bars can be increased to the levels that are required in high speed experiments.

A cover encloses the rotating disk and bar assembly, thus creating a sealed cavity containing the bars. This sealed cavity is needed to prevent the leakage that would occur if the cavity were opened to the exit plenum, i.e., to the exit conditions. A cross section of the high speed bar passing rig is shown in Fig. 1 along with a photograph taken looking toward the inlet.

For the current study, the bars are made of 0.41 mm diameter hypodermic tube. The bar passing frequency is 3600 Hz, providing a reduced frequency for this cascade of $f_r=0.43$, approximately the same as an upstream stator [12]. The ratio of bar diameter to chord, i.e., 1.48%, matches that used for the low speed experiments by Zhang et al. [6] (1.5%) and by Vera et al. [7] (1.3%). The design value for the pitch to chord ratio is 0.784.

The static pressures upstream and downstream of the cascade are measured using 0.3 mm diameter wall pressure tappings. Three conventional Pitot's tubes, upstream of the row of bars, measure the inlet stagnation pressure. The inlet stagnation temperature is measured using a thermocouple placed within the inlet duct upstream of the test section.

A calculation procedure is used to evaluate the mixed-out conditions downstream of the bars. This calculation procedure and its validation are presented by Vera et al. [12]. It is based on the measurement of the drag coefficient of the bars. The drag coefficient has been evaluated at different Mach and Reynolds numbers and a look-up table is used to find the drag coefficient for each operating point. In the present work, this procedure has been validated again by comparing the results obtained with this approach to the direct experimental evaluation of the losses generated by the rotating bars. The cascade was removed and the stagnation pressure was measured by traversing a probe in the pitchwise direction at the same axial location as the leading edges of the blades. The stagnation pressure distribution obtained with a traverse downstream the rotating bars did not show any difference. The change in stagnation pressure across the bars, which is due to viscous losses and viscous work input, is between two and three times smaller than the loss of the cascade.

The cascade consists of nine blades. Adjustable bleed slots were placed on the top and bottom walls at the inlet of the cascade in order to control the flow periodicity. These are shown in Fig. 1.

The profile losses were evaluated using the data from a pitchwise traverse. The traverse plane is located one-half of an axial chord downstream of the trailing edge plane of the cascade. The traverses extended across the wakes of all of the vanes. The losses have been evaluated using the central two blades. A fixed direction four-hole Neptune probe, similar to the one used by Sieverding and Maretto [13] was used to measure the exit flow field (Fig. 1). The local flow conditions at the exit were determined from the calibration curve of the probe. The Mach number, flow angle, and stagnation pressure were used to provide the mixed-out values that were used to calculate the profile loss coefficient. The mixed-out values were determined using a constant area mixing calculation.

All pressures were measured using a 16-channel Scanivalve DSA type 3017. The DSA had a range of 2.5 psid. A reference absolute pressure was provided using a Druck DPI 520 pressure controller. The accuracy of pressure measurements acquired with the DSA 3017 is ± 17 Pa at full-scale. However the DSA has a resolution of approximately 2 Pa. The stagnation pressure at the inlet, before the rotating bars, was used as reference pressure for all the transducers. Therefore, because of the low pressures in this experiment, the resolution of DSA effectively determines the accuracy of the loss data. The kinetic energy loss coefficient was calculated with an accuracy of about 0.1% of the exit dynamic pressure at the design condition ($Re_3=30.000$). It can be seen in Fig. 1 that the DSA has been placed inside the pressurized wind tunnel. This is because the slope of the calibration of a transducer alters when the pressure inside the transducer is significantly different to that outside of the unit.

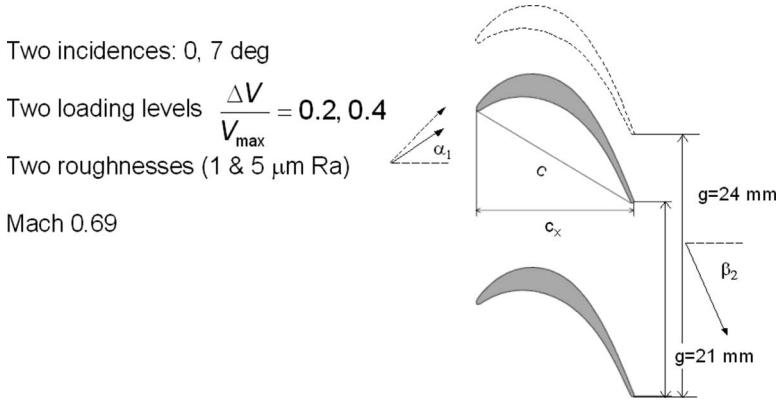

Fig. 2 H2 airfoil schematic

All the traverses were repeated more than three times. The variation in the kinetic energy loss coefficient was less than 1% of the loss.

Hot wire boundary layer traverses were performed over the rear part of the suction side, at 19 locations between 45% and 95% surface length. At each position, the boundary layer traverses consist of 13 points exponentially distributed normal to the wall. The boundary layer traverses were performed up to a distance of 1.0 mm from the wall. The first point close to the wall was at a distance of about 0.02 mm. The location of the wall was found with the method described by Hodson [14]. This process was performed at the operating conditions to account for the aerodynamic lifting of the probe and the small vibrations of the probe support. To take into account the effects of heat transfer to the blade surface, the still-air correction method of Cox [15] was used.

The hot wire boundary layer traverses were carried out using a DANTEC 55P15 boundary layer probe with 5 μm$\times$1 mm platinum-plated tungsten wire. The hot wire was operated in the constant temperature mode, using an overheat ratio of 1.8. A total of 128 ensembles were acquired at each point of the measurement grid. Each ensemble consists of 1024 points logged at 65 kHz, corresponding to about 16 points for each wake passing. In the current experiment, the frequency response of the hot wire is only one order of magnitude greater than the wake passing frequency. In addition the calibration of a hot wire in a compressible flow is a function of the Mach and Reynolds numbers [7]. To be able to use the calibration map, it is assumed that the static pressure and stagnation temperature are constant across the boundary layer. These assumptions are reasonably valid in steady attached flows. The presence of unsteadiness and flow separation compromises the validity of these assumptions suggesting that the results presented should only be used to provide a qualitative picture of the flow field rather than a quantitative one.

The profile used in this test is the H2 airfoil. This is a high-lift airfoil, with an exit velocity and a diffusion factor similar to profile *H* of Curtis et al. [4]. Two different loading levels have been compared, increasing the pitch of about 15% (Fig. 2). The geometry of the cascade is given in Table 1.

The airfoils are manufactured using a wire cutting electrodischarge machining (EDM). The first surface roughness investigated was obtained with a single pass of the wire. The average roughness level is 5 μm. The second airfoil was manufactured with four passes of the wire and the resulting roughness is about 1 μm.

The surface quality was evaluated using an optical interferometer. The value of Ra considered in this study is defined as the arithmetic mean of the absolute departures of the roughness profile from the mean line.

In Fig. 3 there is a comparison of the nondimensional roughness level of the H2 profile with the results of the previous investigation of the HSU2 by Vera et al. [7]. The values are normalized by the axial chord of the airfoil. The highest level is like a cast surface, the lowest is like a polished one.

In order to achieve the low Reynolds numbers required for these tests, the blades have a small chord of 27 mm. The operating conditions of the cascade are provided in Table 2.

The trailing edge thickness of the blades is 0.41 mm. Due to the small size of the blades and the need to preserve the surface finishes, it was not possible to instrument the blades with surface static pressure tappings.

Table 1 Cascade geometrical parameters

Parameter	Unit	Value
Chord, C	(mm)	27
Design inlet flow angle, α_1	(deg)	36.9
Design exit flow angle, β_2	(deg)	−59.04
Aspect ratio, AR	-	3.78
Trailing edge thickness	(mm)	0.41
Pitch/chord, S/C	-	0.784, 0.896
Number of blades	-	9, 8
Surface roughness Ra/(C_x 1000)	-	0.185, 0.037
Axial distance bar to cascade l.e.	(mm)	20

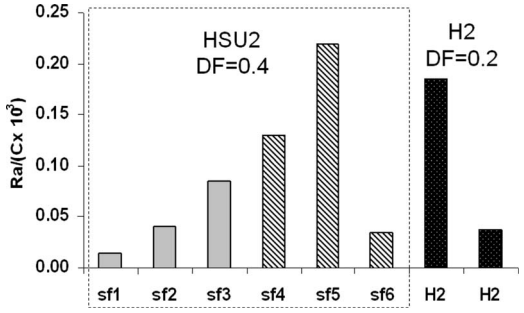

Fig. 3 H2 roughness compared to Vera et al. [9]

Table 2 Cascade operating conditions

Parameter	Unit	Value
Exit Reynolds number	-	30,000–145,000
Inlet Mach number	-	0.36
Exit Mach number, averaged	-	0.69
Reduced frequency, f_r	-	0.43
Incidence, I	(deg)	0, +7

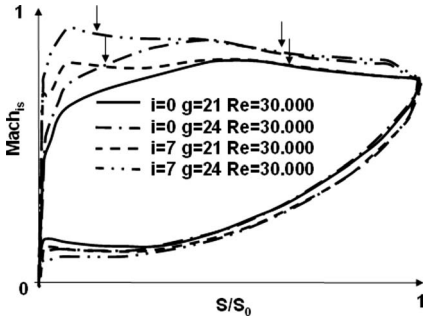

Fig. 4 Isentropic Mach number distribution on H2, MISES calculations, $Re_3=30,000$

3 Profile Design

To design the blade, the 2D solver MISES [16] has been used. Figure 4 presents four computations of the isentropic Mach number distribution with two incidence angles (0/+7 deg) and two pitches (21/24 mm). The incidence is defined as zero at nominal conditions.

All the calculations in Fig. 4 are at the same Reynolds number, i.e., Re=30,000 and at the same exit Mach number, i.e., Mach =0.69, without imposed transition on the suction side. The nominal condition is shown by the continuous line. The airfoil is a forward loaded profile with the peak Mach number at about 45% S_0 in the design case (zero incidence, 21 mm of pitch). The loading distribution of H2 follows the design approach suggested by Coull et al. [11] for low Reynolds number airfoils. Coull et al. [11] studied different velocity distributions on a flat plate with incoming wakes. Their results show that a forward loaded aerofoil has lower losses than an aft loaded one with the same amount of suction side diffusion. In particular, they found that the laminar separation bubble on the suction side produces less loss and is more likely to be suppressed by the wake passing in the case of the forward loaded aerofoil. They also found that the losses began to increase significantly at diffusion factors above 0.2. For this reason the H2 aerofoil has been forwarded loaded with a diffusion factor of about 0.2 and the suction peak at 45% S_0.

Figure 4 above shows that when increasing the incidence angle (dashed line) the rear part of the suction side remains almost unaltered. Only the front half of the profile is affected. The presence of an extra diffusion part on the front side of the blade can generate an earlier transition layer on the suction side with consequently higher losses.

By doubling the diffusion rate on the blade at nominal conditions (dot dashed line) the airfoil becomes naturally more forward loaded. As shown by Coull this has a beneficial effect on the losses. Conversely at positive incidence (double dot dashed line), most of the suction side has an adverse pressure gradient, increasing the risk of an early transition.

The two-dimensional MISES code has been coupled to a prescribed unsteady intermittency model (PUIM) [17] to locate the transition onset and the intermittency distribution. PUIM is an in-house code that uses the freestream distribution of turbulence and the boundary layer data, in this case from MISES. Several correlations are available to predict the transition onset location and the spot production rate. In this case, Mayle's correlation [18] has been used.

Without wake passing, MISES-PUIM predicts a separation region located on the rear part of the suction side in all the cases. In particular, the effect of incidence does not affect the transition location on the suction side with steady inflow. This suggests that the profile losses are almost unaffected by positive incidence (Table 3).

By using a time varying inlet turbulence distribution, it is possible to use PUIM to predict the transition onset with unsteady inflow and how the wake passing alters the transition location on the suction side. A freestream turbulence level of 0.5% was specified and the wake was modeled using a Gaussian distribution with a peak turbulence level of 10% in the center of the wake. The simulations showed that with positive incidence, the wakes could promote an early transition in the first decelerating region as highlight by the black arrows in Fig. 4. As shown in Fig. 4 the Mach distribution at positive incidence is relatively flat downstream of the leading edge, and so the wake induced turbulent boundary layer will remain turbulent along the remainder suction side. This is expected to have a significant effect on the losses, especially at higher Reynolds number. Based on the simulation at the design point $Re_3=30,000$, MISES-PUIM predicts an increase in the losses of about 11% with positive incidence due to the earlier transition of the suction side.

Table 3 Separation and transition position at $Re_3=30.000$ with steady inflow

Case	Separation S/S_0	Transition S/S_0
$i=0$, $g=21$ mm	0.76	0.84
$i=7$, $g=21$ mm	0.75	0.83
$i=0$, $g=24$ mm	0.61	0.68
$i=7$, $g=24$ mm	0.60	0.68

The blades used for the experimental measurements have an average trailing edge thickness of 0.41 mm with a maximum variation of 4%. For the central blades, which were used for the loss evaluation, a difference of less than 1% has been measured.

The contribution of the trailing edge losses to the kinetic energy loss coefficient has been numerically investigated using MISES. The H2 profile has been modified on the pressure side by increasing the thickness of the trailing edge by 20%. The suction side retained the same isentropic Mach number distribution. The losses increased by about 2% at $Re_3=30,000$ and about 5% at $Re_3=120,000$. The dependency on the Reynolds number is due to the fact that at the highest Reynolds numbers, the momentum and displacement thickness of the suction side boundary layer decrease, and consequently the contribution of trailing edge losses increases. These results indicate that the observed variations in the trailing edge thickness have a minor effect on the results shown in this paper.

4 Results

4.1 Design Wake Traverse. The kinetic energy loss coefficient of the profile has been calculated according to

$$\mathrm{KSI}=1-\frac{\frac{1}{2}V_3^2}{\frac{1}{2}V_{3,is}^2}=\frac{T_{s3}-T_{s3,is}}{T_{01}-T_{s3}}=\frac{\left(\frac{P_{s3}}{P_{01}}\right)^{\gamma-1/\gamma}-\left(\frac{P_{s3,is}}{P_{01}}\right)^{\gamma-1/\gamma}}{1-\left(\frac{P_{s3}}{P_{01}}\right)^{\gamma-1/\gamma}}$$

where states 1, 3, and 3,is represent the inlet, the mixed-out exit, and the isentropic exit conditions, respectively.

The normalized kinetic energy loss coefficient of the blade is shown in Fig. 5. The data are presented against the Reynolds number for steady and unsteady inflow conditions at the design exit Mach number of 0.69. The normalization is obtained using the losses of high-lift blade *H* presented by Curtis et al. [4] at $Re_3=130,000$ under unsteady inflow with $f_r=0.78$. In this way the data are directly comparable with the other studies available in the open literature such as those reported in Fig. 5 from Ref. [7].

It is possible to relate the reductions in specific fuel consumption to the changes in the two-dimensional losses presented in this work. By considering the large aspect ratio (AR) of low pressure turbines (LPTs) in modern engines, 80% of overall losses are due to two-dimensional profile losses. By reducing the two-dimensional losses by 10%, the efficiency of LPT rises by about

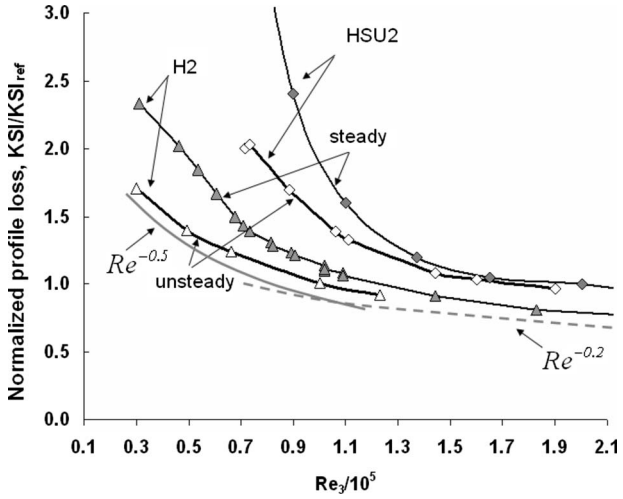

Fig. 5 KSI for steady and unsteady inflows, *i*=0 deg, Ra =5 μm

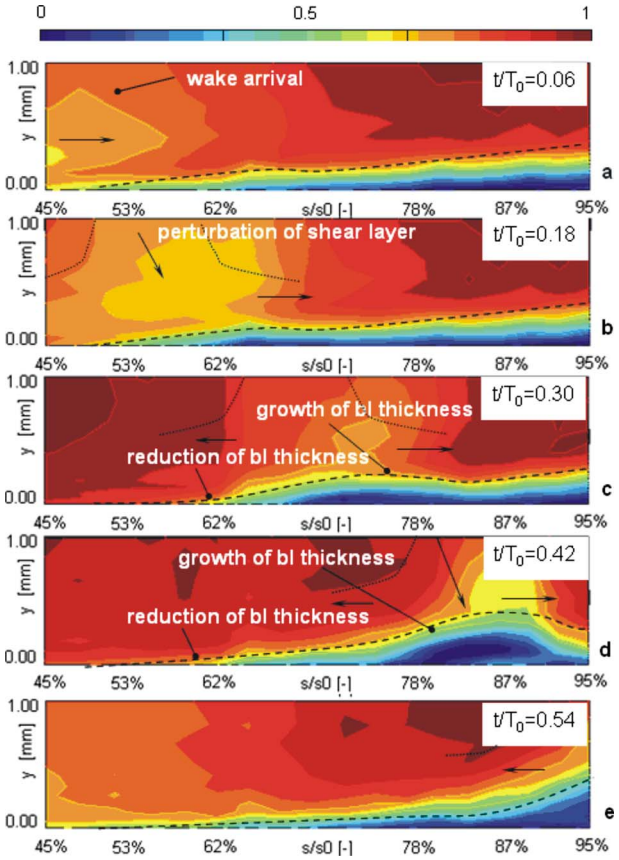

Fig. 6 Ensemble average velocity magnitude on the suction side from 45% S_0 to 95% S_0, Re=30.000, *i*=0 deg, *g*=21 mm, unsteady inflow

0.5% according to Curtis et al. [19]. By using the results in Ref. [8], this generates a reduction in specific fuel consumption (SFC) of about 0.35% in today's engines.

All the losses shown in Fig. 5 were obtained at 0 deg of incidence, with the design pitch. The lines with white symbols represent the results obtained with unsteady inflow. The lines with triangles, (Ra=5 μm) are representative of a surface obtained using a casting process. The lines with diamonds refer to a previous investigation reported by Vera et al. [7] for the HSU2 blade, which was tested at a similar exit Mach number, i.e., Mach$_3$=0.64, with the same inlet and exit angles. The case chosen for comparison is that which produced the lowest losses with incoming wakes. The roughness level is similar despite the fact that HSU2 uses a ribbed surface.

Profile H2 has been studied at lower Reynolds numbers than HSU2. This is due to the new vacuum system of the high speed wind tunnel, which achieves a lower Reynolds number by further reducing the air density. Comparing the losses of H2 (Ra =5 μm) and HSU2 at Re$_3$=200,000 with steady inflow shows that there is a loss increment of about 20%. This is mainly due to the different diffusion factors of two blades. In the case of HSU2, it is about 0.44. Profile H2 has a diffusion factor of about 0.2 at the nominal pitch.

Regarding the as-cast roughness level of profile H2, a reduction in the losses due to the wake passing is shown in Fig. 5. By comparing the as-cast surface with steady and unsteady inflows, a reduction of about 22% is seen at Re$_3$=30,000, and 8% at Re$_3$ =120,000 with unsteady inflow. This is equivalent to a reduction in SFC of, respectively, 0.77% and 0.28%. As suggested by Schulte and Hodson [3] this reduction in losses is due to the earlier transition induced by the wake passing, suppressing, or reducing the laminar separation on the suction side. At lower Reynolds numbers with unsteady inflow, HSU2 exhibits a larger increment in loss when compared with H2. At Re$_3$=90,000, the difference is about 66%.

Curves representing fully laminar flow (Re$^{-0.5}$) and fully turbulent flow (Re$^{-0.2}$) are also presented in Fig. 5, the absolute levels of which have been arbitrarily chosen. Comparing the experimental data with the laminar curve indicates that the loss production mechanism is dominated by the laminar boundary layer at lower Reynolds number under unsteady inflow. This has been confirmed with a more detailed analysis of the suction side boundary layer.

4.2 Hot Wire Measurements. In order to confirm that at the lower Reynolds numbers, the loss production at zero incidence is driven mainly by a laminar separation and the effects that the wakes have upon this, a hot wire was used to measure the boundary layer on the suction side of the H2 profile with a surface roughness of Ra=5 μm at a Reynolds number of Re$_3$=30,000. The reader is reminded that the hot wire results shown in this paper are only qualitative.

The raw velocity data have been phase-locked averaged and are presented in Fig. 6 at different time instants. The time step used in Fig. 6 is $t_{step}=3/50\ T$, where $T=1/f$ and f is the wake passing frequency. The colors correspond to the magnitude of velocity field scaled by the value of the time-mean velocity in the freestream at each surface distance. The x-axis is the suction side surface length divided by the suction side overall length. The traverse extends from about 45% to 95%. The y-axis is perpendicular to the blade surface. The traverse has been done with a clustering toward the wall. On the y-axis, the label indicates the real distance from the wall.

The boundary layer in Fig. 6(a) represents the state of the suction side just before the wake arrives in the traverse domain. The black dashed line is an approximate graphical representation of the boundary layer thickness. In Fig. 6(b), it is possible to observe that the thickness of the boundary layer is reduced from between about 45% and 55% S_0. Given the position of the wake in Fig. 6(a), this is due to the arriving wake, which accelerates the flow close to the surface, reducing the thickness of the boundary layer.

As the wake moves downstream, it passes over the inflexional boundary layer and it promotes a strong interaction, as detected in Figs. 6(c) and 6(d). It is possible to observe two different effects. When the wake passes over the first part of the suction side, from about 45% to about 60%, there is a reduction in the boundary layer thickness. When it passes over the rear part there is the generation of an extended region with low velocity. This behavior

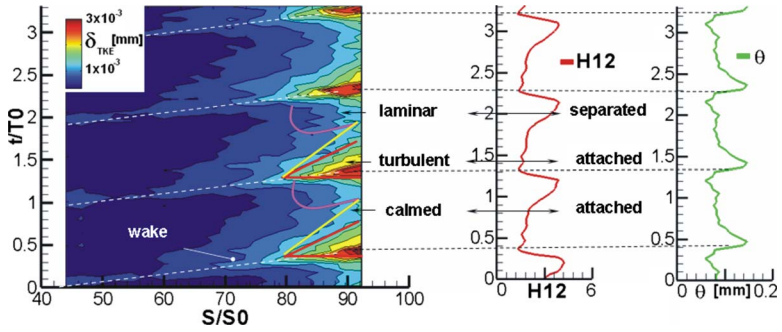

Fig. 7 (Left) s-t diagram of TKE thickness; (Right) θ and H12 at trailing edge, Re=30.000, i=0 deg, g=21 mm, Ra=5 μm, unsteady inflow

appears to be indicative of a roll-up mechanism similar to that described by Stieger and Hodson [20] due to the interaction between the wake and an inflexional boundary layer. After the wake has passed (Fig. 6(*e*)) the boundary layer displacement thickness is reduced, and in the velocity contours there is no evidence of a separation bubble. At this low Reynolds number, the suppression of the laminar separation due to the wake passing seems the most important phenomenon relating to the loss reduction.

To identify the location of the wake, the perturbation field, not shown in this paper, has been evaluated. The velocity perturbation vectors are defined as the time averaged vector field minus the instantaneous one. The velocity defect associated with the wake then appears as a negative jet as described by Meyer [21]. It is negative because the perturbation is directed toward the source of the wake. Close to the suction surface the wake centerline is approximately normal to the wall, and in the perturbation field this appears as a jet pointing toward the surface. When the wake impinges on the suction side, the local pressure variation induced by the wake generates an acceleration of the boundary layer downstream of the impingement point and a deceleration upstream. In the perturbation field this is equivalent to a jet impinging on a surface that splits into two perturbation streams: one pointed downstream along the blade and the other upstream along the blade. The approximate location of the wake is indicated in Fig. 6 with two arrows indicating how the negative jet splits when it impinges on the suction side.

In order to understand if this interaction is related to a laminar or turbulent boundary layer, the phase-averaged Blackwelder parameter in the form of a distance-time diagram is shown in Fig. 7. The Blackwelder parameter is the integral of the root mean square (RMS) fluctuations through the boundary layer nondimensionalized by the boundary layer edge velocity. It is defined as

$$\delta_{\mathrm{TKE}} = \frac{1}{U_{98}^2} \int_{y=0}^{\delta_{98}} \frac{1}{2} (\overline{u'^2} + \overline{v'^2}) dy$$

and represents where on the profile the turbulence is active inside the boundary layer. In this case only one component of velocity has been measured. In the distance-time diagram, the white dashed lines indicate approximately the position of the center of the wake.

To understand if the boundary layer is separating under unsteady inflow, the shape factor at the 92% S_0 is also shown in Fig. 7. The momentum thickness distribution is also shown to highlight the losses production mechanism. Both are derived from the phase-averaged velocity. The high values of shape factor at 92% S_0 show that on the rear part of the suction side, an open separation occurs between the consecutive wakes, as shown in Fig. 6(*a*).

When the wake passes over the separated shear layer, there is a rapid reduction in the shape factor associated with wake induced transition and reattachment. The distance-time diagram shows a high level of turbulence in the boundary layer confirming that the wake is promoting an attached turbulent boundary layer. At the same time the wake induces the rollup of shear layer through the Kelvin–Helmholtz instability, detected in Figs. 6(*c*) and 6(*d*). These structures are not detected in the distance-time diagram of Fig. 7, but the high level of momentum thickness evident at 92% S_0 immediately after the wake centerline, is probably associated with the extra mixing induced by the breakdown of the rollup vortex. A similar trend has been found by Coull et al. [11] in low speed conditions.

The distance-time diagram of Fig. 7 shows that at about 70% S_0 there is an increase in the level of δ_{TKE}, along the path associated with the wake passing, which is indicated by the dashed white lines. Upstream of 70% S_0, the Blackwelder parameter δ_{TKE} is low throughout the cycle, indicating that the boundary layer in this region is laminar and is only slightly affected by the wake passing. Downstream of this point, it is possible to distinguish a triangular region with a high level of turbulence. The low shape factor at 92% S_0, and indeed at other surface locations (not shown), indicates that the boundary layer in this region is attached.

The calmed region that follows, in time, the attached turbulent region is identified by the simultaneously low level of δ_{TKE} and the attached boundary layer, as indicated by the low shape factor. Hence the unsteady wakes cause the boundary layer to remain attached for around 2/3 of the period before the separation starts to grow again. Thus, the beneficial effect of the wake passing at very low Reynolds number, which occurs by the suppression of a laminar separation, is clearly visible. Figure 7 was obtained at a reduced frequency of 0.43. At reduced frequencies above about 0.65, it is likely that there would be no separated flow at the trailing edge.

4.3 Effect of Surface Roughness. The results shown until this point are related to the as-cast surface finish. But it becomes interesting to evaluate what happens if the blade is polished because the reader is reminded that in low pressure turbines used in industrial engines, the blades are polished. The effect on the losses is shown in Fig. 8. The line with white circles indicates the losses of H2 with a polished surface and unsteady inflow. The other lines are the same as in Fig. 5.

By comparing the two cases with unsteady inflow but different surface finishes (lines with white circle and white triangles), it is evident that over a wide range of Reynolds numbers, there is a beneficial effect associated with the rougher surface. The higher roughness level is promoting an earlier transition of the suction side boundary layer, thereby reducing the size of the separation bubble. These observations are consistent with the work of Hourmouziadis and Hofmann [22] that correlates the maximum bubble thickness with the losses. Moreover, using an as-cast finish reduces the manufacturing costs by removing the polishing operation.

According to the open literature [23,24], an important parameter in the case of transition induced by roughness elements is the local Reynolds number based on the roughness height. The rough-

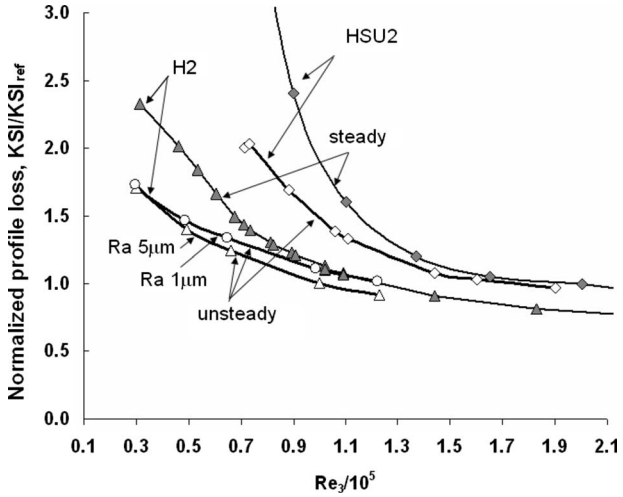

Fig. 8 KSI for steady and unsteady inflows, i=0 deg, Ra =5,1 μm

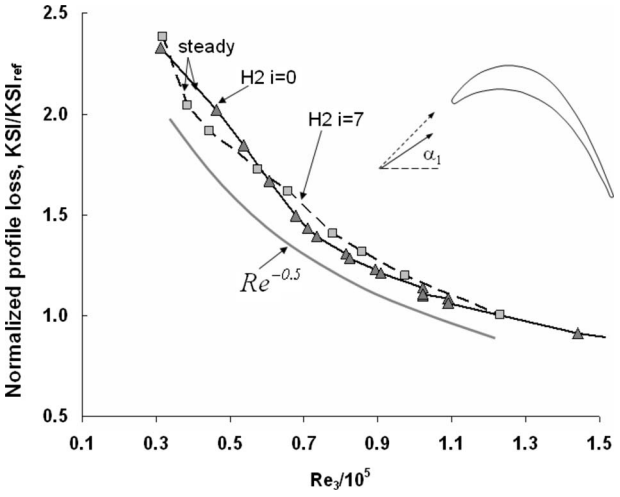

Fig. 9 KSI for steady inflow, i=0/+7 deg, Ra=5 μm

ness Reynolds number for the as-cast surface at Re_3=30.000 is about Re_k=5 with $k_s \approx$Ra. As shown by Roberts and Yaras [25], the effects of roughness spacing and shape are small in comparison to that of the roughness height. The roughness Reynolds number gives an indirect measure of the portion of the boundary layer affected by the roughness element. At a higher Reynolds number, the same roughness element has a greater effect on the transition because it affects a greater part of the boundary layer. This is confirmed in Fig. 5, where the beneficial effect of a rougher surface decreases as the Reynolds number decreases so that at Re_3 =30,000, the two roughness curves intersect. Below this value both surfaces are hydraulically smooth. A possible improvement maybe obtained using a higher roughness level and/or anisotropic surface roughness, e.g., spanwise ribs. The main advantage of such anisotropic roughness is related to the introduction of 2D disturbances parallel to the direction of flow, which are more effective in triggering transition [7].

Due to the fragility of the rotating bars, the unsteady experiments do not extend to the highest Reynolds numbers. Following Refs. [5,6], which showed that the optimum roughness level depends on the Reynolds number, it can be expected that the loss curves corresponding to the two roughness levels tested here will eventually cross. This is because there are two main contributors to the loss: the thickness of the separation bubble on the suction side and the amount of suction surface covered by turbulent as opposed to laminar boundary layer. At the higher Reynolds numbers, the boundary layer on a smooth surface will transition earlier, and a higher roughness level merely serves to create additional loss.

4.4 Effect of Incidence. As suggested by the isentropic Mach number distributions in Fig. 4, the incidence has a strong effect on the suction surface. To evaluate the effect of positive incidence on the losses, a new inlet duct was used to produce an incidence angle of +7 deg. The plane of the rotating bars remained parallel to the cascade inlet plane. The exit Mach number was again 0.69.

The lines of Fig. 9 represent the losses with steady inflow. Under steady inflow conditions, the losses at 0 deg and +7 deg of incidence have very similar values in the Reynolds number range studied. This is consistent with the MISES computations (see Fig. 4), which suggested that the boundary layer remain almost unaltered by the positive incidence. The curve representing fully laminar flow ($Re^{-0.5}$) is also presented in Fig. 9. Comparing the experimental data with the fully laminar curve indicates that the loss production mechanism is dominated by the laminar boundary layer over much of the range of the Reynolds number. This suggests that the flow is still laminar after the second suction side peak and that the leading edge spike at positive incidence is not able to promote an earlier transition on the suction side.

In Fig. 10, there is a comparison of nominal and positive incidences with and without the wake passing. As before the lines with white symbols represent the losses with unsteady inflow.

With unsteady inflow and positive incidence, (dashed line with white squares), the wake passing reduces the losses for Re_3 $<$80,000 when compared with the steady inflow case (dashed line with gray squares). Increasing the Reynolds number above 80,000 means that there is a detrimental effect connected to the wake passing. Above this Reynolds number, the size of the separation bubble is probably reduced, and the main source of loss is connected to the higher portion of the suction side covered by turbulent flow. A confirmation comes from the comparison of the losses of H2 at i=7 deg to the laminar and turbulent trends. Under unsteady inflow, the losses follow the laminar trend for Re_3 $<$80,000. At higher Reynolds numbers, the losses follow a turbulent trend, suggesting that the major source of losses is related to the increased portion of suction side covered by turbulent boundary layer. This was expected given the results of the Mises computation. The experimental data showed that under unsteady inflow at Re_3=30,000, there is an increment of about 11% moving from nominal to positive incidence. The same increment has been predicted using MISES-PUIM.

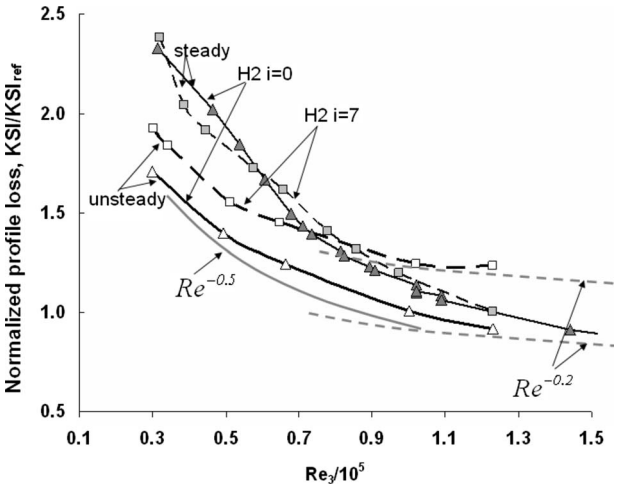

Fig. 10 KSI for steady and unsteady conditions, i=0/+7 deg, Ra=5 μm

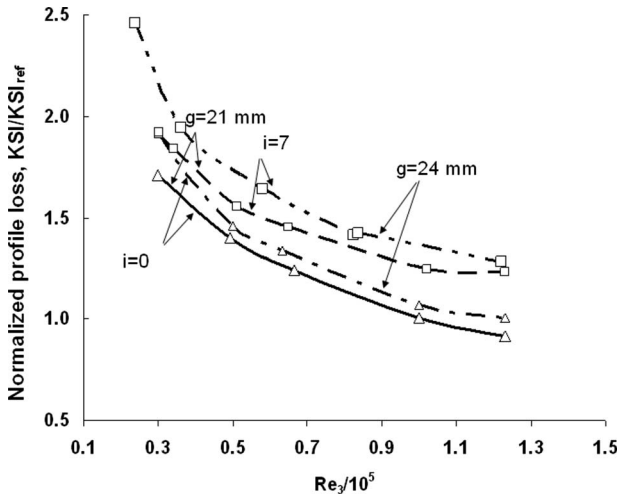

Fig. 11 KSI for steady and unsteady conditions, *i*=0/+7 deg, Ra=5 μm, *g*=21/24 mm

4.5 Effect of Pitch/Chord Ratio. In Fig. 11, the normalized losses are plotted against the Reynolds number for different incidences and loading levels. All of the cases are for unsteady inflow. The steady isentropic Mach number distributions relating to these four cases are shown in Fig. 4. Comparing the loss increment due to positive incidence at a pitch of 24 mm, it is seen that at the lowest Reynolds number, i.e., $Re_3=30{,}000$, the increment is about 8%.

Increasing the pitch, the blade becomes naturally more front loaded. As shown by Coull et al. [11], this has a beneficial effect on the losses because despite a higher diffusion rate, 0.4 instead than 0.2, the diffusion gradient on the suction side is reduced. What we found experimentally is that this is valid at nominal incidence but it generates higher losses with positive incidence and unsteady inflow.

For higher Reynolds numbers $Re_3=120{,}000$, it is about 20%. A similar increment in losses has been found with the design pitch when varying the incidence. This suggests that the same mechanism is involved. In both cases the positive incidence induces an earlier transition on the boundary layer on the front of the blade with unsteady inflow.

5 Conclusions

In the present work, a high-lift low pressure turbine blade has been experimentally investigated. The Reynolds number range is below the values of previous studies. Different surface roughness levels have been compared at two incidence angles and cascade pitches.

The experimental campaign shows that the beneficial effect of wake passing on loss occurs even down to the lowest Reynolds number tested ($Re_3=30{,}000$). The comparison of the present results with laminar trends suggests that the main mechanism of loss formation is related to the laminar boundary layer separation bubble. At the lowest Reynolds number, the hot wire measurements on the suction side show that the interaction between the wakes and the inflexional boundary layer on the suction side is associated with a rollup mechanism similar to that found by Stieger and Hodson [20].

A comparison of the profile losses of blades with two surface roughnesses shows that there is a beneficial effect associated with the rougher surface. In particular, the as-cast surface finish has a better performance over a wide range of Reynolds number. The use of as-cast surface finishes in low pressure turbines is made possible by removing the polishing operation. However the beneficial effect of the roughness decreases with the Reynolds number. A possible improvement may be obtained with a higher level of roughness. At Reynolds numbers higher than that used in the present investigation, i.e., during the take off, it is possible that the roughness has a negative or null effect on the losses.

At positive incidence, the losses with steady inflow are almost the same as at zero incidence. The numerical simulations suggest that this is because the boundary layer on the rear part of the suction side is almost identical in both cases with only slightly different locations of the separation bubble and of the transition point.

With unsteady inflow and positive incidence, the laminar separation bubble is still the major source of losses at the lower Reynolds number. However at higher Reynolds numbers ($Re_3 > 80{,}000$) and with unsteady inflow, the dominant losses mechanism appears to be an increase in the portion of the suction side covered by a turbulent boundary layer. The effect of incidence variations has to be taken into account during the design process.

Acknowledgment

The authors would like to thank Rolls-Royce Plc. for the funding of the project and the permission to publish this paper.

Nomenclature

C = true chord
f = bar passing frequency
f_r = reduced frequency, $f^*(C/V_2)$
α = inlet angle
β = exit angle
i = incidence
g = pitch
S_0 = surface length
Re = Reynolds number based on chord
Re_k = roughness Reynolds number, k_s/C Re
k_s = equivalent sand roughness
Ra = mean peak to valley roughness, $1/N\sum_{i=1}^{N}(h_p-h_v)$
P = pressure
T = temperature
ρ = density
R = gas constant
Mach = Mach number
V = velocity
KSI = kinetic energy loss coefficient
δ_{TKE} = Blackwelder parameter
H_{12} = shape factor, δ^*/θ
θ = Momentum thickness
δ^* = displacement thickness
$\overline{u'}, \overline{v'}$ = velocity variance components

Subscripts

0 = stagnation
1 = inlet conditions
2 = exit conditions from the cascade
3 = mixed-out exit conditions
S = static

References

[1] Vazquez, R., Cadrecha, D., and Torre, D., 2003, "High Stage Loading Low Pressure Turbines. A New Proposal for an Efficiency Chart," ASME Paper No. GT2003-38374.
[2] Hourmouziadis, J. 1989, "Aerodynamic Design of Low Pressure Turbines," AGARD Lecture Series, Paper No. 167.
[3] Schulte, V., and Hodson, H. P., 1998, "Unsteady Wake-Induced Boundary Layer Transition in High Lift LP Turbines," ASME J. Turbomach., **120**(1), pp. 28–35.
[4] Curtis, E. M., Hodson, H. P., Banieghbal, M. R., Denton J. D., Howell, R. J., Harvey, N. W., 1996, "Development of Blade Profiles for Low Pressure Turbine Applications," ASME Paper No. 96-GT-358.
[5] Zhang, X. F., and Hodson, H. P., 2003, "Parametric Study of Surface Rough-

ness and Wake Unsteadiness on a Flat Plate With Large Pressure Gradient," Tenth ISUAAAT, Durham, NC, Sept. 7–11.
[6] Zhang, X. F., Vera, M., Hodson, H. P., and Harvey, N., 2005, "Separation and Transition Control on an Aft-Loaded Ultra-High-Lift LP Turbine Blade at Low Reynolds Numbers: Low-Speed Investigation," ASME Paper No. GT2005-68892.
[7] Vera, M., Zhang, X. F., Hodson, H. P., and Harvey, N., 2005, "Separation and Transition Control on an Aft-Loaded Ultra-High-Lift LP Turbine Blade at Low Reynolds Numbers: High-Speed Validation," ASME Paper No. GT2005-68893.
[8] Lukachko S.P., and Waitz I.A., 1997, "Effects of Engine Aging on Aircraft NO_x Emissions," ASME Paper No. 97-GT-386.
[9] Roman, K. M., and Howell, R., 2007, "Development of Extended Ultra High Lift Low Pressure Turbine Blades Using Selective Roughness and Wake Unsteadiness," Aeronaut. J., **111**, pp. 257–266.
[10] Bloxham, M., Reimann, D., Crapo, K., Pluim, J., and Bons, J. P., 2007, "Synchronizing Separation Flow Control With Unsteady Wakes in a Low-Pressure Turbine Cascade," ASME Paper No. GT2007-27529.
[11] Coull, J. D., Thomas, R. L., and Hodson, H. P., 2008, "Velocity Distributions for Low Pressure Turbines," ASME Paper No. GT2008-50589.
[12] Vera, M., Hodson, H. P., and Vazquez, R., 2003, "The Effect of Mach Number on LP Turbine Wake-Blade Interaction," Tenth ISUAAAT, Durham, NC, Sept. 7–11.
[13] Sieverding, C., and Maretto, L., 1974, "Design and Calibration of Four Probes for Using in the Transonic Cascade Testing," von Karman Institute, Technical Note 100.
[14] Hodson, H. P., 1984, "Measurements of Wake-Generated Unsteadiness in the Rotor Passages of Axial Flow Turbines," ASME Paper No. 84-GT-189.
[15] Cox, R. N., 1957, "Wall Neighbourhood Measurements in Turbulent Boundary Layers Using Hot-Wire Anemometer," A.R.C. Report No. 19101.
[16] Drela, M., and Youngren, H., 1998, "A User's Guide to MISES 2.53," MIT Fluid Dynamics Research Laboratory, Cambridge, MA.
[17] Vilmin, S., Savill, M. A., Hodson, H. P., and Dawes, W. N., 2003, "Predicting Wake-Passing Transition in Turbomachinery Using a Intermittency-Conditioned Modelling Approach," 33rd AIAA Fluid Dynamics Conference and Exhibit, Orlando, FL, Jun.
[18] Mayle, R. E., 1991, "The Role of Laminar—Turbulent Transition in Gas Turbine Engines," ASME J. Turbomach., **113**, pp. 509–537.
[19] Curtis, E. M., Hodson, H. P., Banieghbal, M. R., Denton, J. D., Howell, R. J., and Harvey, N. W., 1997, "Development of Blade Profiles for Low-Pressure Turbine Applications," ASME J. Turbomach., **119**(3), pp. 531–538.
[20] Stieger, R. D. and Hodson, H. P., "The Transition Mechanism of Highly-Loaded LP Turbine Blades," ASME Paper No. GT2003-38304.
[21] Meyer, R.X., 1958, "The Effects of Wakes on the Transient Pressure and Velocity Distributions in Turbomachines," ASME J. Basic Eng., **80**, pp 1544–1552.
[22] Hourmouziadis, J., and Hofmann, G., 2006, "Response of Separation Bubble to Velocity and Turbulence Wakes: Workshop on Unsteady Flows in Turbomachinery," NASA, Report No. NASA/CP/2006-214484.
[23] Koch, C. C., and Smith, L. H., 1976, "Loss Sources and Magnitudes in Axial Flow Compressors," ASME J. Eng. Power, **98**(3), pp. 411–424.
[24] Flack, K. A., Schultz, M. P., and Connelly, J. S., 2007, "Examination of a Critical Roughness Height for Outer Layer Similarity," Phys. Fluids, **19**, p. 095104.
[25] Roberts, S. K., and Yaras, M. I., 2005, "Effect of Surface-Roughness Geometry on Separation-Bubble Transition," ASME Paper No. GT2005-68664.